An Uncertainty-driven and Observability-based State Estimator for Nonholonomic Robots

Daniele Fontanelli, Farhad Shamsfakhr, David Macii
DII – University of Trento, Trento, Italy
E–mail: daniele.fontanelli@unitn.it

Luigi Palopoli
DISI – University of Trento, Trento, Italy
E–mail: luigi.palopoli@unitn.it

***Abstract*—The problem addressed in this paper is the localisation of a mobile robot using a combination of on-board sensors and Ultra-Wideband (UWB) beacons. By using a discrete-time formulation of the system's kinematics, we identify the geometric conditions that make the system globally observable and cast the state estimation problem into the framework of least-square optimisation. The observability filter thus obtained is remarkably different from classic Bayesian filters, such as the Kalman Filter, since it does not need a-priori stochastic models of process and measurement uncertainty contributions and thus proves to have better performance than the Kalman filters if such contributions are partly unknown or differ from the expected values. A second important outcome of this work is the analytical study of the uncertainty propagation. The effectiveness of the designed filter, the validity of the theoretical analysis of estimation uncertainties and the comparisons with a state-of-the-art extended Kalman filter (EKF) are corroborated by extensive simulations and are validated experimentally.**

I. Introduction

Accurate robot positioning is essential for its correct navigation [1]. Unfortunately, in indoor scenarios the Global Positioning System (GPS) signals are not strong enough to provide ubiquitous localisation. Therefore, a number of alternative technological solutions have to be used for robot position tracking. They include (but are not limited to) power fingerprinting of Wi-Fi signals [2], detection of radio frequency identification (RFID) tags [3], [4], computer vision techniques using both natural [5] and artificial landmarks [6]–[8], and Light Detection and Ranging (LiDAR) sensors [9]. Particularly relevant to this paper are the multilateration solutions that exploit the distance measured from a set of wireless nodes (briefly referred to as *anchors* in the following [10]), with a known position in a given reference frame. The distance from each anchor node can be estimated indirectly from the Received Signal Strength Indication (RSSI) values [11], [12] or from the Time-of-Arrival (ToA), the Time-Difference-of-Arrival (TDoA) or Round-Trip Time (RTT) of messages exchanged between each anchor node and the wireless transceiver installed on the robot.

Some of the most promising wireless solutions for indoor localisation rely on Ultra-Wideband (UWB) signals [13]. The key advantage of UWB-based ranging is that the ToA or RTT values can be measured at a low level with a much higher accuracy and precision than using other wireless technologies. As a result, the uncertainty associated with distance measurements is in the order of a few centimetres. Moreover, the recent availability of new-generation smaller and low-cost transceivers offering decimeter-level accuracy (e.g., the DecaWave DW1000 [14]) has lowered the adoption barriers for this technology.

Indoor localisation is subject to two conflicting requirements: on one hand, in many applications planar positioning uncertainty should be at most in the order of a few centimetres, with an orientation uncertainty in the order of a few degrees. On the other, the infrastructural cost and its maintenance (which heavily depends on the number of anchor nodes deployed) should be kept as low as possible. With these considerations in mind, it becomes imperative to understand: i) how to provide accurate localisation with the smallest possible number of anchors; ii) how to merge the dead-reckoning information from low-cost proprioceptive sensors (e.g., inertial measurement units or odometers) with a variable (and sometimes sporadic) amount of distance values from the wireless anchor nodes within the detection range of the transceiver installed on the robot; iii) how to evaluate the overall localisation uncertainty in order to meet desired performance requirements.

The first issue is tightly related to the observability problem: i.e., deciding if the unknown state of the robot can be reconstructed from a time series of measured quantities that are also functions of the system state. Similar observability studies have been proposed in the past for collaborative localisation [15] and for leader–follower formations [16]. Examples of observability analyses for localisation problems are also reported for instance in [7], [17]. However, most of these results are *local*, meaning that they guarantee the convergence of the estimated state to the actual one only if the initial estimate is close enough. This paper instead builds on previous results on global observability [18], which ensure convergence of the estimated state to the actual one for any initial estimate of the state. The main benefit of a global observability analysis is that it can be used to define a dynamic state estimator, namely a filter, that reconstructs, in a finite time, the robot's state (i.e., its position and orientation) from a finite sequence of measurements.

The second and third issues above hinge on the fusion algorithm adopted to merge dead-reckoning sensor data (which suffer from unbounded uncertainty growth) with the distance measures from the detected wireless anchor nodes. Data fusion is often performed through Extended Kalman Filters (EKF) or Unscented Kalman Filters (UKF) [19]. However, such filters require to know the stochastic properties of both the process noise and the random measurement uncertainty contributions affecting the sensor data, otherwise they rely on additional sensors [20], or on a bank of filters [21]. The structure of

the observer adopted in this paper directly emanates from the observability study: we collect the measured data over a number of discrete–time steps and set up the sensor fusion problem in terms of least–square optimisation. Contrary to the Kalman Filtering schemes such as the EKF or the UKF, this solution does not require any prior knowledge of the covariance of the measurement uncertainty contributions. Even if the accuracy of our estimates is comparable with the accuracy of a properly tuned EKF, in practice it may happen that process or measurement uncertainty contributions in real operating conditions differ from those determined during the preliminary uncertainty characterisation step. In such a case, our approach returns much better results than the EKF since it is actually employed in suboptimal conditions. This problem is further stressed by the nonlinearity of both the system and the measurement models. This paper complements and extends the results of a previous conference paper [22] in several respects. First, a revised notation for the discrete–time evolution of the system is adopted to simplify the subsequent analysis. Second, we provide a closed-form expression of state estimation uncertainty when a two-step filter based on the proposed global observability analysis is applied to an arbitrary number of wireless anchor nodes. Such analytical expression of localisation uncertainty closely matches the outcome of several Montecarlo simulations. This result sets the basis for studying the uncertainty propagation over multiple steps, which is the third innovative aspect introduced in this paper. Importantly, this study reveals the existence of two conflicting effects and an optimal trade-off solution in the choice of the number of past measurements that should be used for system state (i.e., localisation) reconstruction. Finally, we report extensive experiments and simulations that provide a conclusive and unequivocal support to all the theoretical findings of this work.

The rest of this manuscript is structured as follows. Section II presents the models and the observability analysis underlying the formulation of the positioning problem. Section III deals with the multi-step estimator design. Section V reports several simulation results to confirm the validity and the good performances of the proposed approach compared with a classic EKF. Section VI reports some experimental results collected on the field. Finally, in Section VII conclusions and the future work directions are outlined.

II. Theoretical Background

In this section, first we present the robot model, and then we subsume the global observability analysis under the assumption that only wireless distance measurements are used for localisation. This analysis stems from simple algebraic manipulations presented in [18] and formalised in [23].

A. Models

Consider a unicycle robot moving according to the following dynamics.

$$\begin{bmatrix}\dot{x}\\ \dot{y}\\ \dot{\theta}\end{bmatrix} = \begin{bmatrix}v\cos\theta\\ v\sin\theta\\ \omega\end{bmatrix}, \tag{1}$$

where $s(t) = [x,\, y,\, \theta]^T$ is the state of the system, θ is the orientation of the vehicle with respect to axis X_w of the reference frame $\langle W\rangle$, v is the robot forward velocity and ω is the robot angular velocity. The vehicle moves across a space instrumented with m wireless anchor nodes (e.g., based on UWB signals), whose coordinates (X_i, Y_i) are known. Assuming that the sampling period of the ranging system is T_s, at each time step kT_s, $k \in \mathbb{N}$, the moving agent collects a set of distance measures. Such values can be gathered into vector

$$\mathcal{Y}_k = \begin{bmatrix}\mathcal{Y}_{1,\,k}\\ \mathcal{Y}_{2,\,k}\\ \dots\\ \mathcal{Y}_{m,\,k}\end{bmatrix} = \begin{bmatrix}\sqrt{(x_k - X_1)^2 + (y_k - Y_1)^2}\\ \sqrt{(x_k - X_2)^2 + (y_k - Y_2)^2}\\ \dots\\ \sqrt{(x_k - X_m)^2 + (y_k - Y_m)^2}\end{bmatrix}. \tag{2}$$

Assuming that during the sampling period T_s the velocities v and ω are held constant (a customary assumption when feedback control is applied), it is possible to find the following discrete–time equivalent dynamics for (1), i.e.

$$\begin{aligned} x((k+1)T_s) &= x(kT_s) + \int_{kT_s}^{(k+1)T_s} v\cos(\theta(\tau))d\tau,\\ y((k+1)T_s) &= y(kT_s) + \int_{kT_s}^{(k+1)T_s} v\sin(\theta(\tau))d\tau,\\ \theta((k+1)T_s) &= \theta(kT_s) + \omega T_s. \end{aligned} \tag{3}$$

Denoting $s((k+1)T_s) = s_{k+1} = [x_{k+1}, y_{k+1}, \theta_{k+1}]^T$ and considering basic trigonometric properties, it follows that

$$\begin{aligned} x_{k+1} &= \begin{cases} x_k + v_k T_s \cos\theta_k & \text{if } \omega_k = 0,\\ x_k + 2\frac{v_k}{\omega_k}\sin\left(\frac{\omega_k}{2}T_s\right)\cos\left(\theta_k + \frac{\omega_k}{2}T_s\right) & \text{otherwise,}\end{cases}\\ y_{k+1} &= \begin{cases} y_k + v_k T_s \sin\theta_k & \text{if } \omega_k = 0,\\ y_k + 2\frac{v_k}{\omega_k}\sin\left(\frac{\omega_k}{2}T_s\right)\sin\left(\theta_k + \frac{\omega_k}{2}T_s\right) & \text{otherwise,}\end{cases}\\ \theta_{k+1} &= \theta_k + \omega_k T_s. \end{aligned} \tag{4}$$

Let us introduce the following symbols, i.e.,

$$\phi_k = \frac{\omega_k}{2}T_s \text{ and } A_k = 2\frac{v_k}{\omega_k}\sin\left(\frac{\omega_k}{2}T_s\right). \tag{5}$$

Given that when $\omega_k \to 0$, then

$$\lim_{\omega_k\to 0} A_k = \lim_{\omega_k\to 0} 2\frac{v_k}{\omega_k}\sin\left(\frac{\omega_k}{2}T_s\right) = v_k T_s,$$

expression (4) simplifies to

$$\begin{aligned} x_{k+1} &= x_k + \Phi_k\cos(\theta_k) - \Psi_k\sin(\theta_k),\\ y_{k+1} &= y_k + \Psi_k\cos(\theta_k) + \Phi_k\sin(\theta_k),\\ \theta_{k+1} &= \theta_k + 2\phi_k, \end{aligned} \tag{6}$$

where $\Phi_k = A_k\cos(\phi_k)$ and $\Psi_k = A_k\sin(\phi_k)$. This simpler formulation than the one adopted in [23] is particularly useful for the multi-step extension proposed in Section IV. Furthermore, for the sake of brevity, the following symbols $\mathbb{S}_k$ and $\mathbb{T}_k$ will be used to denote if, at time step k, the robot moves straight (i.e., $\omega_k = 0$) or if it moves along a curvilinear path (i.e., $\omega_k \neq 0$), respectively.

B. Observability analysis

In this section, we will show that the measurement data gathered into $\mathcal{Y}_k$ up to time kT_s from a given number m of wireless anchor nodes can be actually use to design a filter able to estimate the robot state s_k. This study can be referred to as a *global observability* analysis. A system is globally observable when its initial state s_0 can be determined without ambiguity from the series of collected measurement data. It is worth noting that, for non-linear systems, observability is not a structural property of the system itself, but rather of its trajectories. Therefore, we will first consider two types of trajectories: 1. rectilinear trajectories ($\mathbb{S}_k, \forall k$), 2. curvilinear trajectories ($\mathbb{T}_k$ for some k). Clearly, if the forward velocity of the robot is $v_k = 0$ (i.e., the robot is still or rotates on the spot), its state will be unobservable regardless of the number of anchors available (indeed, the orientation angle θ cannot be estimated). Therefore, we will henceforth assume that $v_k \neq 0, \forall k$.

A first simple result with just one wireless anchor node is subsumed in the following:

Theorem 1: Consider a robot with kinematic (4), output function (2) and $m = 1$ that moves with non-null forward velocity $v_k \neq 0$. The system state is unobservable for any trajectory.

The proof can be readily obtained by simply noticing that for any rotation of the vehicle trajectory with centre in the anchor position, even if the ranging uncertainty is negligible, the set of measurement data is the same, which implies that the trajectory is actually unobservable.

When $m = 2$ anchor devices are available, observability depends on the type of trajectory followed, as subsumed by the following Theorem.

Theorem 2: Consider a robot with kinematic (4), output function (2), $m = 2$ that moves with non-null forward velocity $v_k \neq 0$. Then:

- If the system follows rectilinear trajectories (i.e., $\mathbb{S}_k, \forall k$), then its state is not globally observable;
- If the system turns twice in a row (e.g. $\mathbb{T}_0\mathbb{T}_1$) then its state is globally observable if $\omega_0 T_s \neq h\pi$, and $\omega_1 T_s \neq h\pi$, for $h \in \mathbb{N}$.

The complete proof of this Theorem can be found in [18]. However, its rationale is quite intuitive, as it stems from the ambiguity generated by the trajectories that are symmetric with respect to the segment joining the two available anchor nodes, as shown Fig. 1 for clarity. Indeed, assuming that the two ranging anchors are in positions $P_1 = [X_1, Y_1]^T$ and $P_2 = [X_2, Y_2]^T$ and the vehicle is following a straight path $\mathbb{S}_k$ from position s_k to s_{k+1}, it turns out that the ranging measurements (2) are $\mathcal{Y}_k = [\|P_1 - [x_k, y_k]^T\|, \|P_2 - [x_k, y_k]^T\|]^T$ at time kT_s and $\mathcal{Y}_{k+1} = [\|P_1 - [x_{k+1}, y_{k+1}]^T\|, \|P_2 - [x_{k+1}, y_{k+1}]^T\|]^T$ at time $(k+1)T_s$. As can be noticed from Fig. 1, the same ranging measurements $\mathcal{Y}_k$ and $\mathcal{Y}_{k+1}$ would have been collected from robot positions $s_k^\star$ and $s_{k+1}^\star$, i.e. lying on the symmetric linear path. This condition holds for an arbitrary number of robot positions and ranging measurements if the path remains linear, i.e. $\forall s_{k+i}, s_{k+i}^\star$ with $i \geq 2$ if the path is $\mathbb{S}_{k+i}$. Therefore, since the state of the system cannot be estimated from an arbitrarily large set of measurements, i.e., the robot's position is not observable.

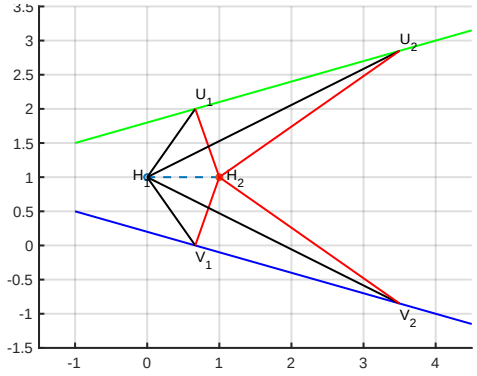

Fig. 1. Motion of the robot along a linear trajectory (green line) and its alias trajectory (blue line), for which the distance values in $\mathcal{Y}_k$, and $\mathcal{Y}_{k+1}$ are the same if ranging uncertainty is negligible.

In practice, the possible ambiguity is reduced to the case of symmetric straight lines. Nonetheless, by using standard results of nonlinear system analysis [24], it is possible to show that the robot state is locally observable [25], as explained in [7] as well. The bottom line of this discussion is that if we use two anchor devices for ranging, the robot can disambiguate its position as far as it turns for at least two time steps.

The use of $m \geq 3$ non-collinear anchor nodes avoids any ambiguity in estimating any trajectory with $v_k \neq 0$, thus enabling global observability if trilateration or multilateration from the anchors is applied twice in a row when the robot is in two different nearby positions. Indeed, as known the Cartesian coordinates (x_k, y_k) of the robot as well as its initial position can be determined from at least three distance values. In particular, given

$$\begin{aligned}\mathcal{Y}_{i,k}^2 &= (x_k - X_i)^2 + (y_k - Y_i)^2 = \\ &= X_i^2 + x_k^2 + y_k^2 + Y_i^2 - 2X_i x_k - 2Y_i y_k,\end{aligned}$$

with $i = 1, \ldots, m$, by subtracting $\mathcal{Y}_{i,k}^2$ from $\mathcal{Y}_{1,k}^2$, i.e. $\Delta_{i,k} = \mathcal{Y}_{1,k}^2 - \mathcal{Y}_{i,k}^2$, we get

$$h_k^{(m)} = 2\Sigma^{(m)} \begin{bmatrix} x_k \\ y_k \end{bmatrix} = \begin{bmatrix} \Delta_{2,k} - X_1^2 - Y_1^2 + X_2^2 + Y_2^2 \\ \Delta_{3,k} - X_1^2 - Y_1^2 + X_3^2 + Y_3^2 \\ \vdots \\ \Delta_{m,k} - X_1^2 - Y_1^2 + X_m^2 + Y_m^2 \end{bmatrix}, \quad (7)$$

where

$$\Sigma^{(m)} = \begin{bmatrix} X_2 - X_1 & Y_2 - Y_1 \\ X_3 - X_1 & Y_3 - Y_1 \\ \vdots & \vdots \\ X_m - X_1 & Y_m - Y_1 \end{bmatrix}. \quad (8)$$

Observe that (7) returns an estimate of the robot planar position (x_k, y_k) provided that the Moore-Penrose pseudo-inverse of Σ is invertible (which is always true if the anchor nodes are not collinear). Finally, the trajectory angle θ_k can be estimated indirectly from (6) once the pair of values (x_k, y_k) and (x_{k+1}, y_{k+1}) in two consecutive positions are

estimated through (7). In particular, if $R(\phi_k)$ denotes the two-dimensional rotation matrix of angle ϕ_k, we have that

$$A_k R(\phi_k)\begin{bmatrix}\cos(\theta_k)\\ \sin(\theta_k)\end{bmatrix} = \begin{bmatrix}x_{k+1}-x_k\\ y_{k+1}-y_k\end{bmatrix}, \tag{9}$$

which finally returns $\theta_k = \arctan\left(\frac{\sin(\theta_k)}{\cos(\theta_k)}\right)$.

III. Two Steps Estimator Design

As briefly explained in the Introduction, the ultimate objective of this work is to design a state estimation filter for robot localisation based on the global observability analysis described in Section II, regardless of the nonlinear nature of both the system dynamic and the measurement model.

In particular, the observability analysis can be used to design a two-step estimator, i.e. an estimator based only on two consecutive records of distance data with $m \geq 3$. This result holds even under the realistic assumption that the linear and angular velocities v_k and ω_k of the robot are affected by additive random contributions ε_k and η_k, respectively, while the wireless (e.g., UWB-based) distance measurement data are affected by random fluctuations modelled by sequence ρ_k. All uncertainty contributions are supposed to be white, with zero mean and variances σ_v^2, σ_ω^2 and σ_ρ^2, respectively. However, the probability density functions of such uncertainty contributions is not relevant for the study at hand. Notice that, for a differential-drive robot like the unicycle in (1), the forward and angular velocities depend linearly on the speed of two independent motors generating the angular wheels velocity ω_r and ω_l the right and left wheel, respectively, i.e. $[v,\omega]^T = F[\omega_l,\omega_r]^T$. Hence, $\sigma_{v\omega} = \mathrm{E}\{\varepsilon_k\eta_k\} \neq 0$.

If the ideal distance between the robot and the i-th anchor node given by (2) at time kT_s, is affected by a random contribution $\rho_{i,k}$, the corresponding measurement result can be modelled as

$$\overline{\mathcal{Y}}_{i,\,k} = \sqrt{(x_k - X_i)^2 + (y_k - Y_i)^2} + \rho_{i,k} = \mathcal{Y}_{i,\,k} + \rho_{i,k},$$

where, both here and in the following, $\bar{\cdot}$ will denote measured quantities. Therefore, from

$$\overline{\mathcal{Y}}_{i,\,k}^2 = \mathcal{Y}_{i,\,k}^2 + \rho_{i,k}^2 + 2\mathcal{Y}_{i,\,k}\rho_{i,k} = \mathcal{Y}_{i,\,k}^2 + \zeta_{i,k}, \tag{10}$$

(where $\zeta_{i,k}$ is a random variable with mean $\mu_{\zeta_{i,k}} = \sigma_\rho^2$ and variance $\sigma_{\zeta_{i,k}}^2 \approx 4\mathcal{Y}_{i,\,k}^2\sigma_\rho^2$ given by the law of propagation of uncertainties [26]), it follows that (7) can be rewritten as

$$\Sigma^{(m)}\begin{bmatrix}\hat{x}_k\\ \hat{y}_k\end{bmatrix} = \frac{1}{2}h_k^{(m)} + \frac{1}{2}\begin{bmatrix}\zeta_{1,k}-\zeta_{2,k}\\ \zeta_{1,k}-\zeta_{3,k}\\ \vdots\\ \zeta_{1,k}-\zeta_{m,k}\end{bmatrix} = \frac{1}{2}h_k^{(m)} + \begin{bmatrix}\nu_{1,2,k}\\ \nu_{1,3,k}\\ \vdots\\ \nu_{1,m,k}\end{bmatrix},$$

where $\hat{\cdot}$ denotes an estimated quantity and $\nu_k^{(m)} = [\nu_{1,2,k}, \nu_{1,3,k}, \ldots, \nu_{1,m,k}]^T$ is a zero–mean random vector with covariance matrix

$$N_k^{(m)} = \sigma_\rho^2\begin{bmatrix}\mathcal{Y}_{1,\,k}^2+\mathcal{Y}_{2,\,k}^2 & \mathcal{Y}_{1,\,k}^2 & \cdots & \mathcal{Y}_{1,\,k}^2\\ \mathcal{Y}_{1,\,k}^2 & \mathcal{Y}_{1,\,k}^2+\mathcal{Y}_{3,\,k}^2 & \cdots & \mathcal{Y}_{1,\,k}^2\\ \vdots & & \ddots & \vdots\\ \mathcal{Y}_{1,\,k}^2 & \mathcal{Y}_{1,\,k}^2 & \cdots & \mathcal{Y}_{1,\,k}^2+\mathcal{Y}_{m,\,k}^2\end{bmatrix}. \tag{11}$$

Of course, if $m \geq 3$, the optimal estimates of the robot position are given by the Weighted Least Squares (WLS) approach, i.e.

$$\begin{bmatrix}\hat{x}_k\\ \hat{y}_k\end{bmatrix} = \frac{1}{2}({\Sigma^{(m)}}^T {N_k^{(m)}}^{-1}\Sigma^{(m)})^{-1}{\Sigma^{(m)}}^T {N_k^{(m)}}^{-1}h_k^{(m)}. \tag{12}$$

The estimation errors are defined with a tilde, i.e. $\widetilde{x}_k = \hat{x}_k - x_k$ and $\widetilde{y}_k = \hat{y}_k - y_k$, and are grouped in the position estimation error vector $\xi_k = [\widetilde{x}_k, \widetilde{y}_k]^T$, whose covariance matrix is

$$\Xi_k^{(m)} = ({\Sigma^{(m)}}^T {N_k^{(m)}}^{-1}\Sigma^{(m)})^{-1} = \begin{bmatrix}\sigma_{x,k}^2 & \sigma_{xy,k}\\ \sigma_{xy,k} & \sigma_{y,k}^2\end{bmatrix}, \tag{13}$$

where

$$\sigma_{x,k}^2 = \frac{\sigma_\rho^{2m-4)}}{g_k}\sum_{i\in\mathcal{I}}\prod_{j=1}^{m-2}\mathcal{Y}_{j,k}^2(Y_{i_{m-1}} - Y_{i_m})^2,$$

$$\sigma_{xy,k} = \frac{\sigma_\rho^{2m-4)}}{g_k}\sum_{i\in\mathcal{I}}\prod_{j=1}^{m-2}\mathcal{Y}_{j,k}^2(X_{i_{m-1}} - X_{i_m})(Y_{i_m} - Y_{i_{m-1}}),$$

$$\sigma_{y,k}^2 = \frac{\sigma_\rho^{2m-4)}}{g_k}\sum_{i\in\mathcal{I}}\prod_{j=1}^{m-2}\mathcal{Y}_{j,k}^2(X_{i_{m-1}} - X_{i_m})^2.$$

Consider that, in the expressions above,

$$g_k = |{\Sigma^{(m)}}^T {N_k^{(m)}}^{-1}\Sigma^{(m)}||N_k^{(m)}|,$$

(with $|M|$ denoting the determinant of a square matrix M), while the set $\mathcal{I}$ in (13) comprises all the permutations of the anchor indexes $\{1,\ldots,m\}$. Thus, one element of $\mathcal{I}$, say $i \in \mathcal{I}$, has elements $i_1, i_2, \ldots, i_m$. Notice also that since $\nu_k^{(m)}$ has zero mean, the elements of ξ_k have zero mean as well, thus ensuring that the filter designed on the basis of (12) is unbiased.

Remark 1: A correct description of the covariance matrix $N_k^{(m)}$ in (11) usually is not available since the actual range distances are unknown. However, we can either assume no knowledge at all (in this case $N_k^{(m)}$ can be replaced by the identity matrix, thus turning the WLS into a standard Least Squares (LS) formulation) or use the measured range value $\overline{\mathcal{Y}}_{i,k}$ in (10) as the best approximation of the actual values $\mathcal{Y}_{i,k}$ that are needed to fill in $N_k^{(m)}$. Observe that, since the range measurement variance σ_ρ^2 acts as a scaling factor of $N_k^{(m)}$, it does not play any role in the estimates of the position $[\hat{x}_k, \hat{y}_k]$. Hence, it is not a tuning parameter of the filter performance.

The estimate $\hat{\theta}_k$ of the orientation angle given by (9) is affected by the uncertainty contributions acting on both ϕ_k and the pair $[\hat{x}_k, \hat{y}_k]$ and $[\hat{x}_{k+1}, \hat{y}_{k+1}]$. More precisely

$$\overline{\phi}_k = \frac{T_s\overline{\omega}_k}{2} = \frac{T_s\omega_k}{2} + \frac{T_s\eta_k}{2} = \phi_k + \alpha_k, \tag{14}$$

where α_k is a zero–mean white noise with variance $\sigma_{\alpha_k}^2 = \sigma_\omega^2 T_s^2/4$. Given the estimated orientation angle

$$\hat{\theta}_k = \arctan\left(\frac{\cos(\overline{\phi}_k)(\hat{y}_{k+1} - \hat{y}_k) - \sin(\overline{\phi}_k)(\hat{x}_{k+1} - \hat{x}_k)}{\sin(\overline{\phi}_k)(\hat{y}_{k+1} - \hat{y}_k) + \cos(\overline{\phi}_k)(\hat{x}_{k+1} - \hat{x}_k)}\right), \tag{15}$$

by computing the first–order Taylor series of (15) at time step k and recalling that the position errors ξ_k and ξ_{k+1} have zero mean, the following approximated expression is derived

$$\hat{\theta}_k \approx \theta_k - \alpha_k + \frac{1}{A_k^2}B_{k+1}\xi_k - \frac{1}{A_k^2}B_{k+1}\xi_{k+1} = \theta_k + \widetilde{\theta}_k, \tag{16}$$

where $B_{k+1} = [y_{k+1} - y_k, -(x_{k+1} - x_k)]$, $A_k^2 = (x_{k+1} - x_k)^2 + (y_{k+1} - y_k)^2$ (see (6)), and $\widetilde{\theta}_k$ is a zero–mean uncertainty term with variance

$$\sigma_{\theta_k}^2 = \frac{\sigma_\omega^2 T_s^2}{4} + \frac{1}{A_k^4} B_{k+1}(\Xi_k + \Xi_{k+1}) B_{k+1}^T, \qquad (17)$$

derived from the fact that ξ_k and ξ_{k+1} are uncorrelated. Moreover, the first term on the right-hand side of (17) is a function of the motion uncertainty σ_ω^2, while the second accounts for the ranging uncertainty σ_ρ^2. Notice that the B_{k+1}/A_k is the unit vector oriented along the direction of motion of the robot. Hence, B_{k+1}/A_k^2 is the direction of motion with magnitude $1/A_k$. Therefore, the smaller A_k (i.e., the smaller the forward velocity v_k or the higher the sampling time T_s in (5)), the higher the orientation angle uncertainty becomes. Observe that $\hat{\theta}_k$, with variance (17), is computed from the measurement data collected at times kT_s and $(k+1)T_s$. Since to design a dynamic estimator like a filter, we need the orientation angle estimate at the same time instant of the last collected measurement, i.e. at $(k+1)T_s$, we can exploit the vehicle dynamic (6) (although affected by uncertainty) to propagate the estimate one step forward, i.e.

$$\hat{\theta}_{k+1} = \hat{\theta}_k + 2\overline{\phi}_k. \qquad (18)$$

As a consequence, the uncertainty contribution $\widetilde{\theta}_{k+1} = \widetilde{\theta}_k + \eta_k T_s$ affecting $\hat{\theta}_{k+1}$ also exhibits zero mean and variance $\sigma_{\theta_{k+1}}^2 = \sigma_{\theta_k}^2 + T_s^2 \sigma_\omega^2$. Observe that $\sigma_{\theta_{k+1}}^2$ is proportional to both the ranging variance σ_ρ^2 and the angular velocity variance σ_ω^2. Finally, the state estimate $\hat{s}_{k+1} = [\hat{x}_{k+1}, \hat{y}_{k+1}, \hat{\theta}_{k+1}]^T$ is affected by an uncertainty contribution $[\xi_{k+1}^T, \theta_{k+1}]^T$, whose covariance matrix is

$$\Gamma_{k+1} = \begin{bmatrix} \Xi_{k+1} & \Xi_{k+1} B_{k+1}^T \\ B_{k+1}\Xi_{k+1} & \sigma_{\theta_{k+1}}^2 \end{bmatrix}. \qquad (19)$$

Remark 2: $\hat{\theta}_{k+1}$ is determined as a function of the estimates $\hat{x}_{k+1}$ and $\hat{y}_{k+1}$. Hence, due to the correlation given by the off-diagonal elements of Γ_{k+1}, the variance $\sigma_{\theta_{k+1}}^2$ will be considered henceforth as a figure of merit for the performance of the filter.

The two-step observability-based filter with $m \geq 3$ anchors can then be designed as follows:

1) Build the matrix $\Sigma^{(m)}$ in (8), set $\hat{\theta}_0$ as the initial guess of the robot orientation, and set $k = 0$;
2) Collect the measurements of the velocities $\overline{v}_k$ and $\overline{\omega}_k$, and compute $\overline{\phi}_k$;
3) Collect the set of measurements $\overline{\mathcal{Y}}_{i,k}$ in (10) at time k and builds the vector of noisy measurements $\overline{\mathcal{Y}}_k$ as in (2). Then, build the vector $h_k^{(m)}$ as in (7) using the noisy ranging measurements $\overline{\mathcal{Y}}_k$;
4) If the LS solution is used (assuming no knowledge about the distribution of uncertainty contributions), set $N_k^{(m)} = I_{m-1}$ (i.e., the identity matrix of dimension $m-1$). Otherwise, use σ_ρ^2 and $\overline{\mathcal{Y}}_k$ to build $N_k^{(m)}$ as in (11);
5) Estimate $\hat{x}_k$ and $\hat{y}_k$ using (12);
6) If $k = 0$, only one set of measurements is available, then go to Step 9. Otherwise, go to the next step;
7) Use (15) to compute $\hat{\theta}_{k-1}$, then apply (18) to finally have $\hat{\theta}_k$;
8) Return the value of $\hat{s}_k = [\hat{x}_k, \hat{y}_k, \hat{\theta}_k]^T$ and the associated covariance matrix Γ_k based on (19);
9) Set $k = k + 1$, then go to Step 2.

As a final comment, we would like to point out that if an LS solution is considered, the statistical characterisation of all the involved standard uncertainties needed to obtain σ_v^2, σ_ω^2, $\sigma_{v,\omega}^2$, σ_ρ^2, is not needed (indeed, the ranging measurements may be affected by different uncertainties, i.e. $\sigma_{\rho_i}^2 \neq \sigma_{\rho_j}^2$, with no effect on the proposed solution). Of course, recalling (19), the actual estimation error is proportional to all the system uncertainties, but their knowledge is not needed to correctly execute the filter. This property is inherited by the multi-step solution which is presented next.

IV. Multistep State Estimator Design

As known, increasing the number of measurements into the Weighted LS estimator reduces the state estimation uncertainty. We now present an extension of the previous solution exploiting all the measurements available not just for steps k and $k+1$ as in Section III, but up to $k+n$. While the position estimates at time step k can still be obtained with (12) only, we are here interested in synthesising the observability-filter to obtain $\hat{\theta}_{k,n}$, that is the estimate of θ_k given all the measurements for n steps ahead. To actually determine the optimal number of backward steps n, we need a closed–form description for the uncertainty affecting $\hat{\theta}_{k,n}$, which is the main objective of what follows. If (4) is applied iteratively for n steps, the following recursive relationship results

$$\begin{bmatrix} x_{k+n} - x_k \\ y_{k+n} - y_k \end{bmatrix} = \sum_{i=0}^{n-1} A_{k+i} R(\Lambda_{k,i}) \begin{bmatrix} \cos(\theta_k) \\ \sin(\theta_k) \end{bmatrix} = D_n \begin{bmatrix} \cos(\theta_k) \\ \sin(\theta_k) \end{bmatrix}, \qquad (20)$$

where $\Lambda_{k,i} = \phi_{k+i} + 2\sum_{j=0}^{i-1} \phi_{k+j}$ is the overall angular variation over i-steps and

$$D_n = \begin{bmatrix} C_n & -S_n \\ S_n & C_n \end{bmatrix} \Rightarrow D_n^{-1} = \frac{1}{|D_n|} \begin{bmatrix} C_n & S_n \\ -S_n & C_n \end{bmatrix},$$

where the components C_n and S_n can be derived from (20) as

$$\begin{aligned} C_n &= \sum_{i=0}^{n-1} A_{k+i} \cos(\Lambda_{k,i}) = C_{n-1} + A_{k+n-1} \cos(\Lambda_{k,n-1}), \\ S_n &= \sum_{i=0}^{n-1} A_{k+i} \sin(\Lambda_{k,i}) = S_{n-1} + A_{k+n-1} \sin(\Lambda_{k,n-1}), \\ |D_n| &= \sum_{i=0}^{n-1} \left[A_{k+i}^2 + 2 \sum_{j=i+1}^{n-1} A_{k+i} A_{k+j} \cos(\Lambda_{k,i} - \Lambda_{k,q}) \right]. \end{aligned} \qquad (21)$$

A useful relation is that by definition $|D_n| = C_n^2 + S_n^2$. Recalling that the bar quantities are computed using measured quantities (hence affected by uncertainties) and by inverting (20), an extended version of (15) can be obtained, i.e.

$$\hat{\theta}_{k,n} = \arctan\left(\frac{\overline{C}_n(\hat{y}_{k+n} - \hat{y}_k) - \overline{S}_n(\hat{x}_{k+n} - \hat{x}_k)}{\overline{S}_n(\hat{y}_{k+n} - \hat{y}_k) + \overline{C}_n(\hat{x}_{k+n} - \hat{x}_k)} \right). \qquad (22)$$

To derive a closed–form expression of the standard deviation of the uncertainties of $\widetilde{\theta}_{k,n} = \hat{\theta}_{k,n} - \theta_{k,n}$, we need to characterise $\overline{C}_n$ and $\overline{S}_n$ in (22). To this end, we first notice the presence of the terms A_k in (21). Therefore, recalling (5) and computing again the Taylor expansion truncated to the first order, it follows that

$$\overline{A}_{k+i} = 2\frac{v_{k+i} + \varepsilon_{k+i}}{\omega_{k+i} + \eta_{k+i}} \sin\left(\phi_{k+i} + \alpha_{k+i}\right) \approx A_{k+i} + \beta_{k+i},$$

where β_{k+i} can be regarded as a zero–mean white sequence with variance

$$\begin{aligned}\sigma^2_{\beta_{k+i}} = & A^2_{k+i}\Bigg[\sigma^2_v + \left(\frac{T_s}{\tan(\phi_{k+i})} - \frac{2}{\omega_{k+i}}\right)\sigma_{v\omega} + \\ & + \left(\frac{1}{\omega^2_{k+i}} + \frac{T_s}{4\tan(\phi_{k+i})^2} - \frac{T_s}{\omega_{k+i}\tan(\phi_{k+i})}\right)\sigma^2_\omega\Bigg].\end{aligned} \tag{23}$$

As a consequence, $\overline{C}_n$ and $\overline{S}_n$ in (22) are affected by the uncertainty terms β_{k+i} and α_{k+i} (which is the one acting on ϕ_{k+i} as reported in (14)), whose covariance is given by

$$\sigma_{\beta_{k+i},\alpha_{k+i}} = \frac{A_{k+i}T_s}{2}\sigma_{v\omega} + \left(\frac{A_{k+i}T_s^2}{4\tan(\phi_{k+i})} - \frac{A_{k+i}T_s}{\omega_{k+i}}\right)\sigma^2_\omega.$$

Since we are considering n steps, we have $i = 0, \ldots, n-1$. By stacking such uncertainty terms in two column vectors, i.e. $\beta_{k,n} = [\beta_k, \ldots, \beta_{k+n-1}]^T$ and $\alpha_{k,n} = [\alpha_k, \ldots, \alpha_{k+n-1}]^T$, and recalling that are both white sequences, their covariance matrix is diagonal and its $(i+1)$-th diagonal element is $\sigma_{\beta_{k+i},\alpha_{k+i}}$.

Therefore, using a first–order Taylor expansion, we have

$$\begin{aligned}\overline{C}_n &\approx C_n + \nabla_\beta C_n \beta_{k,n} + \nabla_\alpha C_n \alpha_{k,n} = C_n + \delta_{C_n}, \\ \overline{S}_n &\approx S_n + \nabla_\beta S_n \beta_{k,n} + \nabla_\alpha S_n \alpha_{k,n} = S_n + \delta_{S_n},\end{aligned}$$

where $\beta_{k,n}$ and $\alpha_{k,n}$ are the vectors of the overall uncertainty contributions affecting $A_k, \ldots, A_{k+n-1}$ and angles $\phi_k, \ldots, \phi_{k+n-1}$ in $\Lambda_k, \ldots, \Lambda_{k+n-1}$, respectively. Hence, the $(i+1)$-th elements of the gradient of C_n (for $i = 0, \ldots, n-1$) with respect to $\beta_{k,n}$ and $\alpha_{k,n}$ are respectively

$$\begin{aligned}(\nabla_\beta C_n)_i &= \cos(\Lambda_{k,i}), \\ (\nabla_\alpha C_n)_i &= -A_{k+i}\sin(\Lambda_{k,i}) - 2\sum_{q=i+1}^{n-1} A_{k+q}\sin(\Lambda_{k,q}), \\ (\nabla_\beta S_n)_i &= \sin(\Lambda_{k,i}), \\ (\nabla_\alpha S_n)_i &= A_{k+i}\cos(\Lambda_{k,i}) + 2\sum_{q=i+1}^{n-1} A_{k+q}\cos(\Lambda_{k,q}).\end{aligned}$$

Therefore, the zero-mean uncertainty term δ_{C_n} affecting C_n is

$$\begin{aligned}\sigma^2_{\delta_{C_n}} &= \sum_{i=0}^{n-1} \sigma^2_{\beta_{k+i}}(\nabla_\beta C_n)^2_i + \sigma^2_{\alpha_{k+i}}(\nabla_\alpha C_n)^2_i + \\ &+ 2\sigma_{\beta_{k+i},\alpha_{k+i}}(\nabla_\beta C_n)_i(\nabla_\alpha C_n)_i = \\ &= \sigma^2_{\delta_{C_{n-1}}} + \sigma^2_{\beta_{k+n-1}}\cos(\Lambda_{k,n-1})^2 + \sigma^2_{\alpha_{k+n-1}}A^2_{k+n-1}\cdot \\ &\cdot \sin(\Lambda_{k,n-1})^2 - A_{k+n-1}\sin(\Lambda_{k,n-1})[2\sigma_{\beta_{k+n-1},\alpha_{k+n-1}} + \\ &+ 4\sum_{i=0}^{n-2}\sigma_{\beta_{k+i},\alpha_{k+i}}\sin(\Lambda_{k,i}) - \sigma^2_{\alpha_{k+i}}\cdot \\ &\cdot (A_{k+n-1}\sin(\Lambda_{k,n-1}) - (\nabla_\alpha C_{n-1})_i)] = \sigma^2_{\delta_{C_{n-1}}} + \Delta^2_{\delta_{C_n}},\end{aligned} \tag{24}$$

which can be similarly obtained for $\sigma^2_{\delta_{S_n}}$ acting on S_n. From this explicit form, it can be noticed that $\sigma^2_{\delta_{C_n}} > \sigma^2_{\delta_{C_{n-1}}}$ and $\sigma^2_{\delta_{S_n}} > \sigma^2_{\delta_{S_{n-1}}}$. Moreover,

$$\begin{aligned}\sigma_{\delta_{C_n},\delta_{S_n}} = & \sum_{i=0}^{n-1}\sigma^2_{\beta_{k+i}}(\nabla_\beta C_n)_i(\nabla_\beta S_n)_i + \\ & + \sigma^2_{\alpha_{k+i}}(\nabla_\alpha C_n)_i(\nabla_\alpha S_n)_i + \sigma_{\beta_{k+i},\alpha_{k+i}}\cdot \\ & \cdot \left[(\nabla_\beta C_n)_i(\nabla_\alpha S_n)_i + (\nabla_\alpha C_n)_i(\nabla_\beta S_n)_i\right].\end{aligned}$$

It is now possible express the estimation error $\widetilde{\theta}_{k,n}$ by using a first order Taylor approximation of (22), that is

$$\begin{aligned}\hat{\theta}_{k,n} \approx \theta_k &+ \frac{S_n}{|D_n|}\delta_{C_n} - \frac{C_n}{|D_n|}\delta_{S_n} + \\ &+ \frac{B_{k+n}}{B_{k+n}B^T_{k+n}}\xi_k - \frac{B_{k+n}}{B_{k+n}B^T_{k+n}}\xi_{k+n} = \theta_k + \widetilde{\theta}_{k,n},\end{aligned} \tag{25}$$

which extends (16) to the multistep case. We can finally generalise the result in (17), noticing that $\widetilde{\theta}_{k,n}$ is a zero-mean random sequence with variance

$$\begin{aligned}\sigma^2_{\theta_{k,n}} = & \frac{S^2_n}{|D_n|^2}\sigma^2_{\delta_{C_n}} + \frac{C^2_n}{|D_n|^2}\sigma^2_{\delta_{S_n}} - 2\frac{S_nC_n}{|D_n|^2}\sigma_{\delta_{C_n},\delta_{S_n}} + \\ & + \frac{B_{k+n}}{(B_{k+n}B^T_{k+n})^2}(\Xi_k + \Xi_{k+n})B^T_{k+n},\end{aligned} \tag{26}$$

where Ξ_k and Ξ_{k+n} are reported in (13). Notice that the first three terms account for the motion uncertainties σ^2_v, σ^2_ω and $\sigma_{v\omega}$, while the last term depends on σ^2_ρ.

All the estimates $\hat{\theta}_{k,i}$ can be averaged together, i.e.

$$\hat{\theta}_k = \frac{1}{n}\sum_{i=1}^{n}\hat{\theta}_{k,i} = \theta_k + \frac{1}{n}\sum_{i=1}^{n}\widetilde{\theta}_{k,i}. \tag{27}$$

Due to the recursive nature of (21), the correlation between $\hat{\theta}_{k,n}$ and $\hat{\theta}_{k,i}$ (for $i = 1, \ldots, n-1$) is not negligible, hence their covariance is

$$\begin{aligned}\sigma_{\theta_{k,i},\theta_{k,j}} = & \frac{S_iS_j}{|D_i||D_j|}\sigma_{\delta_{c_i},\delta_{c_j}} - \frac{S_iC_j}{|D_i||D_j|}\sigma_{\delta_{c_i},\delta_{s_j}} + \\ & - \frac{C_iS_j}{|D_i||D_j|}\sigma_{\delta_{s_i},\delta_{c_j}} + \frac{C_iC_j}{|D_i||D_j|}\sigma_{\delta_{s_i},\delta_{s_j}} + \\ & + \frac{B_{k+i}}{B_{k+i}B^T_{k+i}}\Xi_k\frac{B^T_{k+j}}{B_{k+j}B^T_{k+j}}.\end{aligned}$$

Therefore, the variance of the estimation error of $\hat{\theta}_k$ is given by

$$\sigma^2_{\theta_k} = \frac{1}{n^2}\sum_{i=1}^{n}\sigma^2_{\theta_{k,i}} + \frac{2}{n^2}\sum_{i=1}^{n}\sum_{j=i+1}^{n}\sigma_{\theta_{k,i},\theta_{k,j}}.$$

By virtue of (24) and (26), we have that $\sigma^2_{\theta_{k,n}} \geq \sigma^2_{\theta_{k,n-1}}$ and unknown. Therefore, if $\sigma^2_{\theta_{k,n}}$ grows with n less than quadratically (which is a quite reasonable assumption), the minimum value of $\sigma^2_{\theta_k}$ will be attained for $n \to +\infty$.

However, if the measurement results up to time $(k+n)T_s$ are used to retrieve $\hat{\theta}_k$, the estimate should be propagated n

steps ahead to obtain $\hat{\theta}_{k+n}$. Therefore, by using the angular velocity values of n subsequent steps, it follows from (6) that

$$\hat{\theta}_{k+n} = \hat{\theta}_k + \sum_{i=0}^{n-1} (\omega_{k+i} + \eta_{k+i}) T_s. \tag{28}$$

Thus, the corresponding variance is

$$\sigma^2_{\theta_{k+n}} = \sigma^2_{\theta_k} + n T_s^2 \sigma^2_\omega. \tag{29}$$

Observe that in (29), while a larger number of steps n reduces $\sigma^2_{\theta_k}$, the term due to σ^2_ω tend to grows linearly. Therefore, an optimal number of steps must exists which minimises (29). Such a value that will be evaluated in the following sections.

Remark 3: When only straight-line trajectories are considered (i.e., if $\omega_k = 0$, $\forall k$), then $\beta_{k,n}$ and $\alpha_{k,n}$ in (25) are uncorrelated. Moreover, (23) simplifies to $\sigma^2_{\beta_k} = T_s^2 \sigma_v^2$. In such a case, a remarkable reduction of $\sigma^2_{\theta_{k,n}}$ can be observed. This fact can be exploited to control the trajectory of the robot in order to achieve the minimum uncertainty associated with θ_k when the observability-based filter is used for localisation.

As reported for the two-step case, the multi-step observability-based filter with $m \geq 3$ anchors can now be derived. In particular, the only difference in this case affects the computation of θ_k, hence Steps 7) and 8) of the two-step case, which are detailed next:

7) If $k < n$, use (22) to compute $\hat{\theta}_{0,i}$, $i = 1, \ldots, k$, then average those results to estimate $\hat{\theta}_0$ by means of (27) and then apply (28) to finally have $\hat{\theta}_k$. Otherwise, if $k \geq n$, use (22) to compute $\hat{\theta}_{k-n,n}$, then average those results to estimate $\hat{\theta}_{k-n}$ by means of (27) and then apply (28) to finally have $\hat{\theta}_k$;
8) Return the value of $\hat{s}_k = [\hat{x}_k, \hat{y}_k, \hat{\theta}_k]^T$ and the associated covariance matrix, which is a function of (29);

V. Simulation Results

The objective of the simulation-based analysis is twofold. First, we want to provide sufficient evidence that the standard uncertainties based on analytical expressions (13) and (17) are actually close to those obtained with Monte Carlo (MC) simulations. For the sake of brevity, only the results for the two-step filter will be reported in the following. Then, the results of further MC simulations are used to evaluate the estimation performance of the proposed observability-based filter compared with a standard EKF.

A. Verification of closed–form estimation uncertainty

To evaluate the correctness of expressions (13) and (17), 100 different initial positions $s_0 = [x_0, y_0, \theta_0]^T$ of the robot and as many anchor locations (X_i, Y_i) with $i = 1, \ldots, m$ and $m = 20$ were generated with uniform distributions within $[\pm 40 \text{ m}, \pm 40 \text{ m}, \pm\pi \text{ rad}]$ and $[\pm 40 \text{ m}, \pm 40 \text{ m}]$, respectively. For each initial configuration, we assumed that $v_k \in (0, 2]$ m/s and $\omega_k \in [-\pi/5, \pi/5]$ rad/s. The sampling period for position estimation is set to $T_s = 100$ ms. One million realisations of the normally distributed and white uncertainty contributions ρ_k, ε_k and η_k were generated assuming that such sequences exhibit zero mean and standard deviations $\sigma_\rho = 0.5$ cm, $\sigma_v = 0.1$ m/s and $\sigma_\omega = 0.1$ rad/s, respectively. Also, the covariance of angular and forward velocity uncertainties is set to $\sigma_{v\omega} = 0.08$ m rad/s^2. Consider that such values are purely indicative, since the purpose of the present simulation-based analysis is to evaluate the correctness of (13) and (17). Fig. 2(a) shows the comparison between the theoretical standard deviations σ_x and σ_y of the robot position uncertainty and $|\sigma_{xy}|$ of (13). In particular, both the theoretical curves of σ_x, σ_y and $|\sigma_{xy}|$ (solid lines) and the corresponding curves resulting from MC simulations (dashed lines with cross markers) are plotted as a function of the number of anchor nodes m. Fig. 2(b) shows a similar comparison between the theoretical behaviour of σ_θ (solid line) and the corresponding simulation-based standard deviation (dashed lines with cross markers). Therefore, (13) and (17) can be regarded as an effective measure of the uncertainties acting on the actual estimation error on the system state $\tilde{s}_k = \hat{s}_k - s_k$ for any given trajectory. In all cases, the simulation results are in excellent accordance with

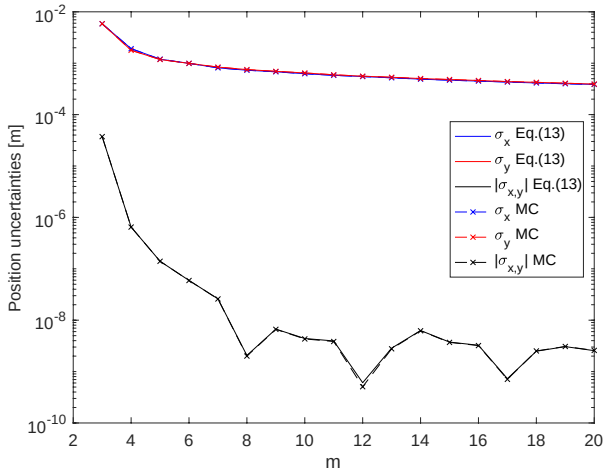

(a)

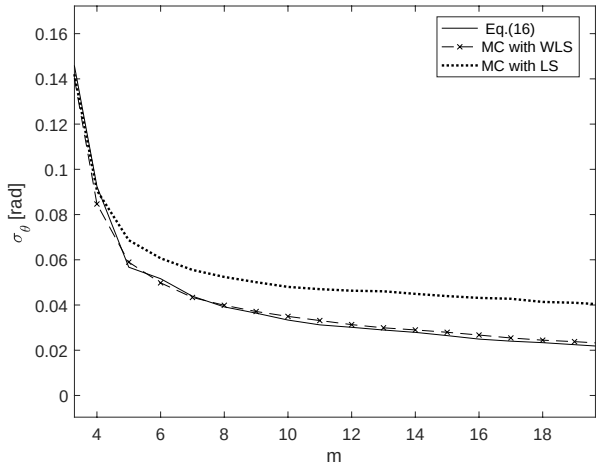

(b)

Fig. 2. Comparison between the theoretical curves (solid lines) and the corresponding simulation-based values (dashed lines with cross markers) of σ_x, σ_y and $|\sigma_{xy}|$ in (a) and of σ_θ in (b), as a function of the available anchor nodes m. A further comparison between Monte Carlo simulations obtained when a plain LS (dotted line) estimator is adopted instead of the WLS (dashed lines with cross markers) is also shown in (b).

the theoretical curves. Moreover, from the same picture, it is possible to see that by increasing m (namely, by increasing the amount of available anchor nodes), state estimation uncertainty improves, as expected. In addition, Fig. 2(b) shows also a slight difference of the estimation uncertainty associated with the orientation angle $\hat{\theta}_k$ when a plain LS filter (dotted line) replaces a WLS filter (which is instead perfectly consistent with the theoretical analysis). This result supports the claim that good estimation performances can be achieved even if no specific information on individual measurement uncertainty contributions is available.

Further results, obtained by considering other potential probability density functions of the measurement uncertainty contributions (e.g., uniformly or Beta-distributed) are quite in accordance with those shown in Fig. 2 and therefore are not shown for the sake of brevity. Such results just confirm the that the performance of the observability-based filter is weakly dependent on the distribution of measurement uncertainty contributions.

B. Performance of the observability-based filter

An additional set of 500 MC simulations was performed to evaluate the estimation uncertainty of the proposed observability-based filter with respect to an EKF implemented with the following equations for the prediction step:

$$\hat{s}_{k+1}^{-} = f(\hat{s}_k, v_k, \omega_k),$$
$$P_k^{-} = F_k P_{k-1} F_k^T + G_k Q_k G_k^T$$

where the superscript $\cdot^-$ denotes the predicted quantities, $f(\hat{s}_k, v_k, \omega_k)$ is reported in (6), $F_k = \frac{\partial f(\hat{s}_k, v_k, \omega_k)}{\partial \hat{s}_k}$, $G_k = \frac{\partial f(\hat{s}_k, v_k, \omega_k)}{\partial [v_k, \omega_k]^T}$ and $Q_k = \begin{bmatrix} \sigma_v^2 & \sigma_{v\omega} \\ \sigma_{v\omega} & \sigma_\omega^2 \end{bmatrix}$. In the update step, we have

$$K_{k+1} = P_{k+1}^{-} H_{k+1}^T \left(H_{k+1} P_{k+1}^{-} H_{k+1}^T + R_{k+1} \right)^{-1},$$
$$\hat{s}_{k+1} = \hat{s}_{k+1}^{-} + K_{k+1} \left(Z_{k+1} - \hat{\mathcal{Y}}_{k+1}(\hat{s}_{k+1}) \right),$$
$$P_{k+1}^{-} = \left(I_3 - K_{k+1} H_{k+1} \right) P_{k+1}^{-},$$

where Z_{k+1} is the set of the m ranging measurements at time $k+1$, $\hat{\mathcal{Y}}_{k+1}(\hat{s}_{k+1})$ is given by (2) once the predicted position estimates $\hat{x}_{k+1}^{-}$ and $\hat{y}_{k+1}^{-}$ are used instead of x_{k+1} and y_{k+1}, $H_{k+1} = \frac{\partial \hat{\mathcal{Y}}_{k+1}(\hat{s}_{k+1})}{\partial \hat{s}_k}$, and $R_{k+1} = \sigma_\rho^2 I_m$.

In the considered scenario, the robot starts from the position $s_0 = [x_0, y_0, \theta_0]^T = [0.2 \text{ m}, 0.4 \text{ m}, 43 \text{ deg}]$. The system evolution was simulated for 20 s with a sampling time $T_s = 100$ ms. The velocity profiles v and ω are piecewise linear. In the first 10 seconds, $v = 3$ m/s and $\omega = -57.3$ deg/s (i.e. $-\pi$ rad/s, clockwise rotation). Between 10 and 15 seconds, the velocities change linearly till reaching $v = 2.4$ m/s and $\omega = 57.3$ deg/s, respectively, (i.e. π rad/s, counterclockwise rotation). Finally, both velocities remain constant for the remaining 5 seconds. Since the simulated robot moves within a large environment, $m = 4$ wireless anchor nodes placed at coordinates $(X_i, Y_i) = (\pm 20, \pm 20)$ (i.e. the corners of a square of 40 m side) are considered to be sufficient for a proper localisation. For each trial, the results obtained with the observability-based filter are compared with those obtained with a standard EKF, under the assumption that all the uncertainty contributions (i.e. ε_k, η_k and ρ_k) are normally distributed, white and with a zero mean. Different values of σ_v, σ_ω and σ_ρ are considered. The variance $\sigma_{\theta_k}^2$ of the orientation estimated with the proposed observability-based filter and with the EKF are reported in Fig. 3.

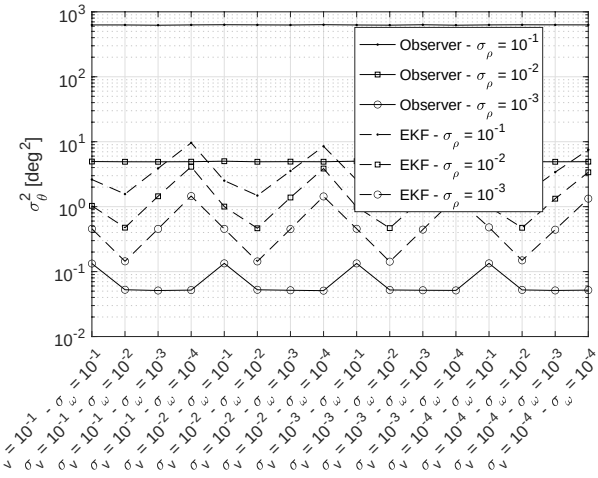

Fig. 3. σ_θ^2 results for different values of σ_v (expressed in m/s), σ_ω (expressed in rad/s) and σ_ρ (expressed in m), for the proposed observability-based filter without any knowledge about the uncertainties (solid line) and for a properly tuned EKF (dashed line).

The chosen scenario is optimal for the EKF, which operates under the effect of known normally-distributed and white uncertainty contributions, while the observability-based filter relies just on the two-step filter defined in Section III, i.e. for $n = 2$, using an LS solution (no a-priori knowledge on the noise is exploited). Of course, the uncertainty of both state estimators is affected by the ranging uncertainty σ_ρ. For large values of σ_ρ ($\sigma_\rho \approx 10^{-1}$ m), the EKF exhibits better performance. For small values of σ_ρ ($\sigma_\rho \approx 10^{-3}$ m) the observability-based filter clearly dominates, while for intermediate values (σ_ρ in the order of cm) the performance of the two solutions is close. The reason of this behaviour is due to the emphasis that the observer gives to the external measurements, whereas the EKF can shift the weight between the internal model and the external measurements according to the relative weight of the process and measurement noise covariances. The results obtained with the EKF deviate from the theoretical ones in the case of small values of σ_ρ due to the errors caused by the system nonlinearities.

The estimation uncertainty of the observability-based filter can be significantly reduced by increasing the number of backward steps n. However, the improvement is non monotonic for the reasons explained in Section IV. In fact, the optimal number of steps depends on σ_ω, as reported in (29) and shown in Fig. 4 for $\sigma_v = 10^{-3}$ m/s, $\sigma_\omega = 10^{-3}$ rad/s $\sigma_\rho = 10^{-1}$ m. In this example, the optimal number of backward steps is $n \approx 20$. It has to be noted that this choice is a distribution-free structural property of the observability-based filter. As shown in the next section, the experimental data exhibit a close match with these theoretical findings.

VI. Experimental Results

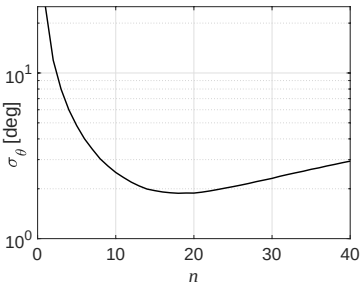

Fig. 4. σ_θ for a variable number of backward steps n when $\sigma_v = 10^{-3}$ m/s, $\sigma_\omega = 10^{-3}$ rad/s $\sigma_\rho = 10^{-1}$ m.

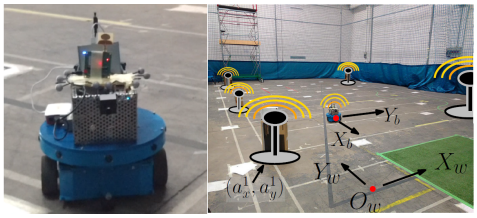

(a)

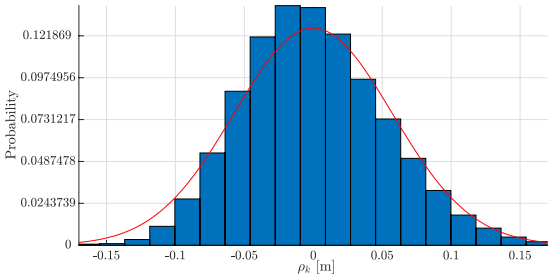

(b)

Fig. 5. (a) Unicycle-like vehicle adopted for the experimental validation and representation of the reference system with the deployment of the UWB anchors, as adopted in [19]. (b) UWB ranging error.

The effectiveness of the proposed observer-based filter is further substantiated and discussed with experiments on an actual robot moving in an environment equipped with 14 OptiTrack cameras covering a 12×8 m^2 area and providing millimetre level localisation at 125 Hz adopted as ground truth. The unicycle-like wheeled robot and the testing area [Fig. 5(a)] are instrumented with DecaWave EVB1000 UWB anchors. These platforms are equipped with an STM32F105 MCU, a DW1000 UWB transceiver, and a PCB antenna. The firmware is implemented atop a Contiki OS. Fig. 5(b) shows the histogram of the UWB-based distance errors. The distribution is approximately Gaussian, with zero-mean and standard deviation $\sigma_\rho = 0.06$ m. In the experimental setup, one UWB platform is placed approximately on top of the centre of the robot. Robot's ego-motion is measured also by two wheel encoders sampled at 50 Hz. The distance between the UWB device on board of the robot and the $m = 5$ anchors is measured through a Single-Sided Two-Way Ranging (SS-TWR) scheme, which is based on the time-of-flight measurement of a two-way message exchange between two UWB nodes at a maximum rate of 200 Hz [27]. However, in the present experimental study the actual rate for position estimation is 50 Hz (i.e., $T_s = 0.02$ s), as in [19]. UWB and odometry data are sent via WiFi to a laptop, which also stores the ground truth data acquired from the OptiTrack vision system. As far as the wheels encoders are concerned, after estimating and compensating the systematic deviations due to the differences between the nominal and actual wheel diameter values on a direct and a circular path, the covariance of the random uncertainty contributions affecting odometry was modelled by using the robot movement increments of the right and left wheels as explained in [1]. In this way, we found that $\sigma_v = 0.1$ m/s and $\sigma_\omega = 0.08$ rad/s.

Four different sample trajectories, named *T1* to *T4*, are considered and depicted in Fig. 6 with a solid black line. Fig. 7 depicts the standard uncertainty σ_θ for the four different trajectories as a function of the number of steps for the multi-step observability filter. From the obtained behaviours, we have chosen an average optimal number of steps $n = 88$. Notice that these curves experimentally validate the simulation results in Fig. 4. The trajectories estimated by the EKF and the LS multistep state observability-based estimator with $n = 88$ steps are plotted in Fig. 6, with red dashed and blue dotted lines, respectively. For a quantitative comparison, the standard localisation uncertainties σ_x, σ_y and σ_θ, are reported in Table I. As a comparison, we report also the WLS solution (i.e., assuming to set the standard uncertainty weights equal to the correct values, as in the EKF case). From this table it is evident that the experimental performance of the three algorithms (namely their accuracy) is quite similar. However, the proposed LS observability-based filter does not embed nor require any prior knowledge on sensor uncertainties. On the contrary, the EKF results obtained with values of σ_v, σ_ω and σ_ρ that are significantly smaller (over-confident) or larger (under-confident) than the respective true standard deviation values resulting from a preliminary sensor characterisation are consistently worse than the results reported in Table I for all the considered trajectories *T1* to *T4*, as expected.

We have paid specific attention to test the robustness of the proposed multi-step estimator by down-sampling the available UWB measurements (i.e. if the UWB sampling frequency decreases from 50 Hz to 1 Hz). As shown in Fig. 8 for the four trajectories, in this situation the EKF may have large errors (red dashed lines) since a larger sampling period implies a change of σ_v and σ_ω that, if not correctly determined, leads to inconsistency. The effect of the nonlinearities in (1) makes the uncertainties associated with larger sampling periods dependent on the particular trajectory considered. However, the proposed multi-step observability-based filter, which heavily relies on the measurements when available, can compensate for this phenomenon, as confirmed by the stability of the estimated trajectories (blue dotted lines in Fig. 8).

Finally, in Table II we report the maximum, minimum and average execution times for a single iteration of the LS and WLS multi-step observability-based filter with $n = 88$ and the EKF. It should be noted that the quantities here reported are obtained for a Matlab implementation executed on a laptop equipped with 2.60-GHz Intel Core i7 microprocessor and 16 GB RAM. The maximum processing times per iteration of all estimators is less than the actual sampling time $T_s = 20$ ms, thus ensuring real–time performances.

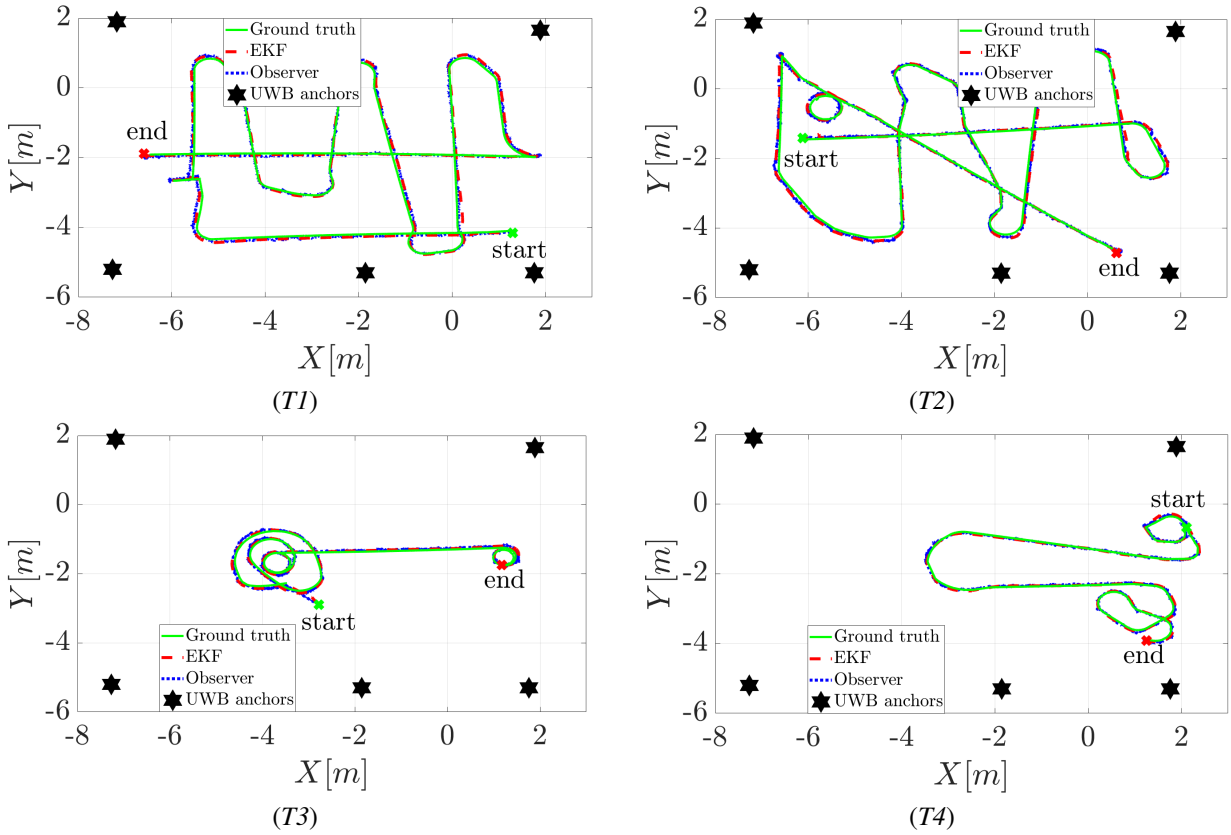

Fig. 6. Actual paths of the robot (solid lines), EKF estimate trajectories (red dashed lines) and paths estimated by the observability-based filter (blue dotted lines) in four cases labelled as *T1–T4*. Both position estimators are qualitative efficient in tracking the trajectory examples.

	EKF				LS				WLS			
	T1	*T2*	*T3*	*T4*	*T1*	*T2*	*T3*	*T4*	*T1*	*T2*	*T3*	*T4*
σ_x [cm]	4.1	4.2	6	2.1	4.8	4.1	6.6	2.6	4.5	4.3	5.3	2.4
σ_y [cm]	4	3.5	6.6	3.3	4.6	3.8	6.7	3.2	4	3.4	4.9	3.2
σ_θ [rad]	0.16	0.17	0.20	0.20	0.18	0.28	0.21	0.45	0.17	0.29	0.20	0.44

TABLE I. AVERAGE STANDARD UNCERTAINTIES OF ROBOT LOCALISATION OBTAINED WITH THE EKF AND THE OBSERVER-BASED FILTER, RESPECTIVELY, (WITH BOTH WLS AND LS SOLUTIONS WITH $n = 88$ STEPS) FOR THE FOUR SAMPLING TRAJECTORIES IN FIGURE 6.

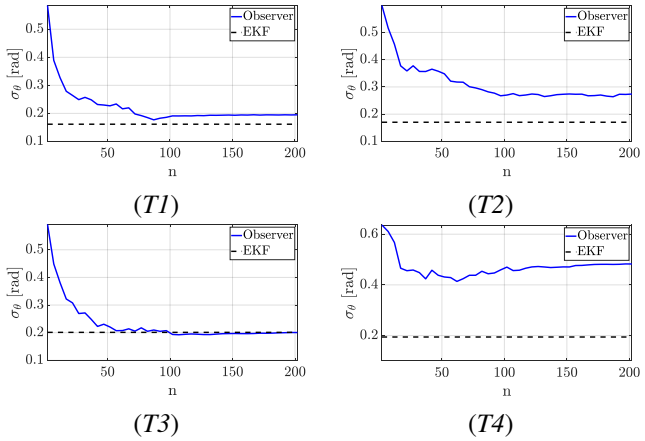

Fig. 7. σ_θ for different values of n (solid lines) along the four trajectories considered and obtained with the LS approach. For comparison, the result attained by the EKF is also reported (dashed line).

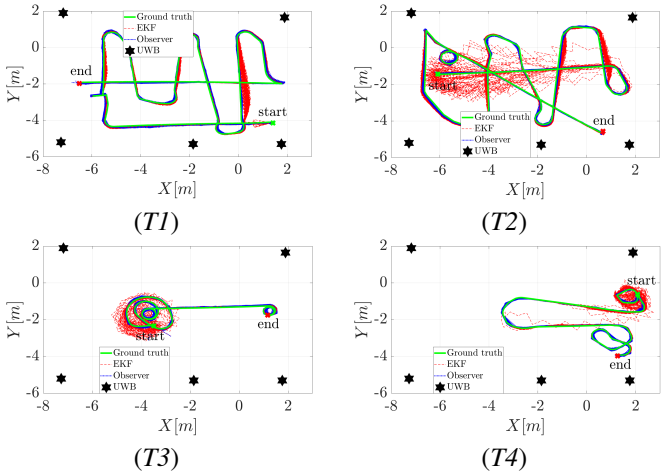

Fig. 8. Tracking errors for the EKF (red dashed line) and the observer-based filter (dotted blue line) with UWB sampling rates ranging from 50Hz to 1Hz.

VII. CONCLUSION

In this paper we have presented a technique for the estimation of the position and orientation of a mobile robot based on the fusion of dead-reckoning data from on-board sensors (e.g., encoders) and distance measurements from a set

	EKF	LS	WLS
Average [ms]	0.05	0.65	2.3
Max [ms]	0.59	1	19
Min [ms]	0.04	0.13	1.7

TABLE II. COMPUTATION TIMES OF A SINGLE ITERATION OF THE EKF, LS AND WLS (FOR THE OBSERVER-BASED FILTER WITH $n = 88$ STEPS) APPLIED TO THE EXPERIMENTAL DATA.

of wireless anchor nodes (e.g. based on UWB signals to ensure higher accuracy). Previous research results have provided conditions for the global observability of the robot state to be estimated. The least-squares estimation technique presented in this paper is a direct derivation of global observability. Unlike Kalman filtering schemes, the proposed solution does not require any specific assumption on the distributions of the measurement uncertainty contributions associated with the sensors employed. is not negatively affected by The analytical structure of the filter lends itself to an elegant analysis of state estimation uncertainty. Moreover, an optimal number of steps that should be considered in the estimation process to minimise positioning uncertainty can be determined. Several simulation and experimental results corroborate and confirm the correctness of the theoretical analysis in all its different parts.

A few points remain open for future work. First, in our scheme the cartesian component of the state are directly derived from the latest distance measurements from the anchors. A possible alternative approach is to set up a least-squares scheme similar to the one used for orientation angle estimation in order to reduce uncertainty. Second, possible spurious or missing distance measurements (e.g., due to the presence of occlusions in the line of sight between the robot and some anchors) could thwart the convergence of the algorithm. The use of robust regression could be a useful tool to tackle this issue. Finally, we could use the proposed localisation technique to set up and solve a Simultaneous Localisation and Mapping (SLAM) problem.

REFERENCES

[1] R. Siegwart and I. R. Nourbakhsh, *Introduction to Autonomous Mobile Robots*. Scituate, MA, USA: Bradford Company, 2004.

[2] P. Chen, Y. B. Xu, L. Chen, and Z. A. Deng, "Survey of WLAN fingerprinting positioning system," *Applied Mechanics and Materials*, vol. 380, pp. 2499–2505, Aug. 2013.

[3] A. Motroni, P. Nepa, V. Magnago, A. Buffi, B. Tellini, D. Fontanelli, and D. Macii, "SAR-based Indoor Localization of UHF-RFID Tags via Mobile Robot," in *International Conference on Indoor Positioning and Indoor Navigation (IPIN)*. Nantes, France: IEEE, Sept. 2018, pp. 1–8.

[4] P. Nazemzadeh, F. Moro, D. Fontanelli, D. Macii, and L. Palopoli, "Indoor Positioning of a Robotic Walking Assistant for Large Public Environments," *IEEE Trans. on Instrumentation and Measurement*, vol. 64, no. 11, pp. 2965–2976, Nov 2015.

[5] B. Dzodzo, L. Han, X. Chen, H. Qian, and Y. Xu, "Realtime 2D code based localization for indoor robot navigation," in *Proc. IEEE Int. Conference on Robotics and Biomimetics (ROBIO)*, Shenzhen, China, Dec. 2013, pp. 486–492.

[6] F. Zenatti, D. Fontanelli, L. Palopoli, D. Macii, and P. Nazemzadeh, "Optimal Placement of Passive Sensors for Robot Localisation," in *Proc. IEEE/RSJ International Conference on Intelligent Robots and System (IROS)*. Daejeon, South Korea: IEEE/RSJ, Oct. 2016, pp. 4586–4593.

[7] V. Magnago, L. Palopoli, A. Buffi, B. Tellini, A. Motroni, P. Nepa, D. Macii, and D. Fontanelli, "Ranging-free UHF-RFID Robot Positioning through Phase Measurements of Passive Tags," *IEEE Trans. on Instrumentation and Measurement*, vol. 69, no. 5, pp. 2408–2418, May 2020.

[8] P. Nazemzadeh, D. Fontanelli, D. Macii, and L. Palopoli, "Indoor Localization of Mobile Robots through QR Code Detection and Dead Reckoning Data Fusion," *IEEE/ASME Transactions on Mechatronics*, vol. 22, no. 6, pp. 2588–2599, Dec. 2017.

[9] M. J. Gallant and J. A. Marshall, "Two-dimensional axis mapping using LiDAR," *IEEE Trans. on Robotics*, vol. 32, no. 1, pp. 150–160, Feb. 2016.

[10] Y. Zhou, Jun Li, and L. Lamont, "Multilateration localization in the presence of anchor location uncertainties," in *2012 IEEE Global Communications Conferenc (GLOBECOM)*, 2012, pp. 309–314.

[11] D. Macii, A. Colombo, P. Pivato, and D. Fontanelli, "A Data Fusion Technique for Wireless Ranging Performance Improvement," *IEEE Trans. on Instrumentation and Measurement*, vol. 62, no. 1, pp. 27–37, Jan. 2013.

[12] D. Giovanelli, E. Farella, D. Fontanelli, and D. Macii, "Bluetooth-based Indoor Positioning through ToF and RSSI Data Fusion," in *International Conference on Indoor Positioning and Indoor Navigation (IPIN)*. Nantes, France: IEEE, Sept. 2018, pp. 1–8.

[13] K. Cheok, M. Radovnikovich, P. Vempaty, G. Hudas, J. Overholt, and P. Fleck, "UWB tracking of mobile robots," in *Proc. IEEE International Symposium on Personal Indoor and Mobile Radio Communications (PIMRC)*, Instambul, Turkey, Sep. 2010, pp. 2615–2620.

[14] DecaWave, "DW1000 Data Sheet," 2016.

[15] G. P. Huang, N. Trawny, A. I. Mourikis, and S. I. Roumeliotis, "Observability-based consistent ekf estimators for multi-robot cooperative localization," *Autonomous Robots*, vol. 30, no. 1, pp. 99–122, 2011.

[16] G. L. Mariottini, G. Pappas, D. Prattichizzo, and K. Daniilidis, "Vision-based localization of leader-follower formations," in *Proceedings of the 44th IEEE Conference on Decision and Control*. IEEE, 2005, pp. 635–640.

[17] S. Cedervall and X. Hu, "Nonlinear observers for unicycle robots with range sensors," *IEEE transactions on automatic control*, vol. 52, no. 7, pp. 1325–1329, 2007.

[18] L. Palopoli and D. Fontanelli, "Global Observability Analysis of a Nonholonomic Robot using Range Sensors," in *European Control Conference (ECC)*, San Petersburg, Russia, May 2020.

[19] V. Magnago, P. Corbalán, G. Picco, L. Palopoli, and D. Fontanelli, "Robot Localization via Odometry-assisted Ultra-wideband Ranging with Stochastic Guarantees," in *Proc. IEEE/RSJ International Conference on Intelligent Robots and System (IROS)*. Macao, China: IEEE, Oct. 2019, pp. 1–7, accepted.

[20] H. Han, J. Wang, F. Liu, J. Zhang, D. Yang, and B. Li, "An emergency seamless positioning technique based on ad hoc uwb networking using robust ekf," *Sensors*, vol. 19, no. 14, p. 3135, 2019.

[21] Y. Xu, Y. S. Shmaliy, C. K. Ahn, G. Tian, and X. Chen, "Robust and accurate uwb-based indoor robot localisation using integrated ekf/efir filtering," *IET Radar, Sonar & Navigation*, vol. 12, no. 7, pp. 750–756, 2018.

[22] L. Palopoli, D. Macii, and D. Fontanelli, "A positioning filter based on uncertainty and observability analyses for nonholonomic robots," in *2020 IEEE International Instrumentation and Measurement Technology Conference (I2MTC)*, 2020, pp. 1–6.

[23] L. Palopoli, D. Macii, and D. Fontanelli, "A Positioning Filter based on Uncertainty and Observability Analyses for Nonholonomic Robots," in *Proc. IEEE Int. Instrumentation and Measurement Technology Conference (I2MTC)*. Dubrovnik, Croatia: IEEE, May 2020, pp. 1–6, available online.

[24] A. Isidori, *Nonlinear control systems*. Springer Science & Business Media, 2013.

[25] A. Bicchi, D. Prattichizzo, A. Marigo, and A. Balestrino, "On the observability of mobile vehicle localization," in *Theory and Practice of Control and Systems*. World Scientific, 1998, pp. 142–147.

[26] BIPM, IEC, IFCC, ILAC, ISO, IUPAC, IUPAP, and OIML, *Evaluation of measurement data Guide to the expression of uncertainty in measurement*. JCGM, Sep. 2008.

[27] Q. Wang, "Analysis of ranging error with high precision and the improved algorithm of UWB," in *Proceedings of the 2020 4th Inter-*

national Conference on Cloud and Big Data Computing, ser. ICCBDC '20, New York, NY, USA, 2020, p. 8185.